BIBECHANA
Vol. 21, No. 2, August 2024, 129-141

ISSN 2091-0762 (Print), 2382-5340 (Online)
Journal homepage: http://nepjol.info/index.php/BIBECHANA
Publisher:Dept. of Phys., Mahendra Morang A. M. Campus (Tribhuvan University)Biratnagar

Adsorption of water on vacancy defected h-BN bilayer at B and N sites

Madhav Nepal[1], Ganesh Paudel[1], Santosh Aryal[1]
Arun Devkota[2], Hari Krishna Neupane[1*]

[1] *Amrit Campus, Tribhuvan University, Kathmandu, Nepal*
[2] *Central Department of Physics, Tribhuvan University, Kathmandu, Nepal*
[*]Corresponding author. Email: hari.neupane@ac.tu.edu.np

Abstract

Two dimensional (2D) materials are used to manufacture the various gadgets. Their properties are therefore appealing. In the present work, we have studied the structural, electronic, and magnetic properties of 2D bilayer hexagonal-Boron Nitride (h-BN), single B vacancy defect on h-BN (B-hBN), single N vacancy defect on h-BN (N-hBN), water adsorption; on B-hBN (w-B-hBN) and on N-hBN (w-N-hBN), materials by spin-polarized density functional theory (DFT) methods employing Quantum ESPRESSO (QE) computational tools. The structural stability of the h-BN, B-hBN, N-hBN, w-B-hBN, & w-N-hBN materials has been investigated by determining their minimum ground state energy and binding energy, and found that they are stable materials. The pristine h-BN bilayer supercell structure is also found to be more compact than other defective configurations. By analyzing the band structures and density of states (DoS) plots of these materials, we have examined their electronic properties, and found that pristine h-BN has a broad bandgap, whereas B-hBN, N-hBN, w-B-hBN, & w-N-hBN exhibit semiconducting nature. The DoS and partial density of states (PDoS) computations of the considered materials are used to study their magnetic properties. It is found that pristine h-BN is a non-magnetic, and B-hBN, N-hBN, w-B-hBN & w-N-BN are magnetic materials. Therefore, vacancy defects on pristine h-BN, and water adsorption on vacancy defected h-BN materials cause it to change from non-magnetic to magnetic. They could find use in the domain of device

Keywords
Adsorption, bilayer, defect, spin states.

Article information
Manuscript received: February 7, 2024; Revised: April 4, 2024; Accepted: April 5, 2024
DOI https://doi.org/10.3126/bibechana.v21i2.62607

1 Introduction

Boron Nitride (BN) stands out as the most lightweight chemical compound within the group III- V in periodic table, having an equal distribution of Boron and Nitrogen atoms [1–6]. It's structure is similar of graphene's structure [7]. Two dimensional (2D) hexagonal Boron Nitride (h-BN) was

constructed by numerous methods including liquid and micromechanical exfoliation, chemical vapor deposition (CVD), and other novel synthetic approaches [8–10]. At room temperature and under ambient pressure, the hexagonal structure stands out as the stable phase among these various structures [11]. h-BN is originally an electrical insulator due to its wide bandgap energy of values in the range of (3.5-6.0) eV obtained from DFT and GW calculations [12, 13]. h-BN is used in various fields such as tunneling devices, chemical sensors, transistors, lubricants due to their wide bandgap energy and various structural characteristics [13–17]. Additionally, it exhibits a high degree of inertness towards a wide range of gas molecules, and it also be easily adjusted using various methods to attain different properties and functions [17–19] This tuning can be achieved through strategies like doping and introducing vacancy defect in the stable structure [19, 20]. The presence of vacancy defect in 2D h-BN material develops the spontaneous magnetization due to the distribution of unequal spin states of electrons in the orbitals of atoms present in the material [15, 21–23].

Boron (B) and Nitrogen (N) atoms in h-BN are strongly covalently bound due to their electronegativity [24]. In the meantime, nearby layers interact with one another by a weak van der Waals (vdWs) force [25]. h-BN is formed a sp^2-hybridization between B & N atoms [26–28]. Furthermore, compared to graphene, h-BN's structure is thermally and chemically stable. It works well as a lubricant because of its lower coefficient of friction [29, 30]. h-BN has a unique set of characteristics, including atomic flatness, incredibly low roughness, and no dangling bonds on its surface [31]. Young's modulus (270 Nm^{-1}) and thermal conductivity (400 $Wm^{-1}K^{-1}$) of 2D h-BN are significantly higher than those of the majority of metals and ceramic materials [32–36].

h-BN bilayer is created by vertically staking two monolayers. Its properties are changed when it placed in a humid environment. Thus, adsorbed water molecules modify its electronic, magnetic, optical, and thermal properties [37–42]. Many investigations have been conducted recently on the adsorption of water molecules on the surface of different other 2D materials. It is found that structural, electronic, and magnetic properties of defected materials are changed due to the adsorption of water molecules [14, 42]. After a thorough analysis of the literature, we found that no studies have been done on the structural, electronic, and magnetic characteristics of water adsorbed on pristine h-BN, and B & N vacancy defected h-BN bilayer materials. In the present work, we have investigated the structural, electronic, and magnetic properties of B & N sites vacancy defected bilayer of h-BN supercell structures (i.e., B-hBN & N-hBN), and water adsorption on these supercell structures (i.e., w-B-hBN & w-N-hBN) respectively, by spin-polarized density functional theory (DFT) methods using the computational tools' Quantum ESPRESSO (QE) codes.

Below is an arrangement of the remaining portions of this manuscript: In the methods and materials section, the procedures and supplies utilized in this investigation are detailed. In the results and discussion section, we present our findings and their interpretations, and in the conclusions section, we express our final thoughts.

2 Material and Methods

The investigation of structural, electronic, and magnetic properties of single B atom vacancy defect on (4×4) bilayer supercell structure of h-BN (B-hBN), single N atom vacancy defect on (4×4) bilayer supercell structure of h-BN (N-hBN), and water molecules adsorbed on B-hBN (w-B-hBN) and N-hBN (w-N-hBN) materials was done using first-principles calculations based on the spin-polarized density functional theory (DFT) method [42]. The Generalized Gradient Approximation (GGA) was utilized using Perdew-Burke-Ernzerhof (PBE) exchange correlations in order to incorporate the electronic exchange and correlation effects in the DFT theory [43]. PBE functional cannot adequately describe the weak van der Waals (vdWs) force present in bilayer supercell structures. Therefore, to determine the type of vdWs interaction between the interlayers of bilayer structures, semi-empirical dispersion correlated density functional theory (DFT-D2) technique is utilized. An effective potential for each atom in a system is used to substitute the complex effects of the motion of an atom's core electrons and its nucleus using Grimme's Rappe-Rabe-Kaxiras-Joannopoulos (RRJK) model of ultrasoft pseudopotentials. So, we have used RRJK model of ultrasoft pseudopotentials and plane wave basis set in the convergence test.

A (4×4) supercell bilayer structure of h-BN is constructed by incorporating 64 atoms, where single layer of h-BN contains 16 B atoms, and 16 N atoms. Single B & N sites vacancy defected h-BN are created by randomly removing 1B & 1N atoms respectively from the upper surface of h-BN supercell structure. In single layer h-BN, B or N vacancy defect of 3.13% is formed, whereas in bilayer h-BN, B or N vacancy defect of 1.56% is produced (i.e., 1B or 1N atom out of 32 BN atoms in single layer). Then, these supercell structures are optimized by calculating their kinetic energy cutoff (ecutoff), lattice parameter (a), and k-points (k-cutoff), through the convergence test. They are found to be 35 Ry, 4.65 Å, and (22×22×1) re-

spectively. These optimized values are taken in the input file for relax calculations. The relax calculations of considered materials have done by using Broyden-Fletcher-Goldfrab-Shanno (BFGS) scheme [44] until the force and total energy change between two successive scf iterations are less than 10^{-3} Ry/Bohrs and less than 10^{-4} Ry, respectively. The optimized and relaxed structures of pristine h-BN, and B & N sites vacancy defected bilayer h-BN are shown in figures-1(a-c) respectively.

Furthermore, water molecule is adsorbed on the defected structures of B-hBN & N-hBN, respectively. Then relax calculations are carried out with the Broyden-Fletcher-Goldfrab-Shanno (BFGS) scheme [43] until the force and total energy minimum values vary between two consecutive scf iterations. These values are likewise found to be less than 10^{-4} Ry and 10^{-3} Ry/Bohrs, respectively. Figures-1(d-e) displays the relax structures of water adsorbed on B-hBN (i.e., w-B-hBN) and on N-hBN (i.e., w-N-hBN) materials, respectively. To assure the accuracy of the results, the Marzarri-Vanderbilt (M-V) smearing method is utilized in the calculations, with a small broadening width of 0.001 Ry [43–47]. For self-consistency, the "David" diagonalization approach with a 0.6 mixing factor is selected. In order to do the band calculations, 200 k-points are chosen along the reciprocal lattice's high symmetry points. The sample locations in the reciprocal lattice's first Brillouin Zone are these k-points. Density of states (DoS) and partial density of states (PDoS) computations are carried out to investigate magnetic properties of materials.

3 Results and Discussion

3.1 Structural Properties

The structural properties of bilayer h-BN material with single B atom vacancy defect, and single N atom vacancy defect; have been examined, along with the effects of water adsorption on these materials. This analysis is conducted by computing the bond length between B-N atoms, binding energy of the systems, interlayer distance of bilayers, and defect generation energies. First, a unit cell of bilayer h-BN material has been created by taking the optimized values of lattice parameter (a) = 4.65 Å, kinetic energy cutoff = 35 Ry, and k-points = 22 in the input file. Then relax calculations are done to get optimized and relaxed unit cell structure of bilayer h-BN. The prepared relaxed unit cell of h-BN is stretched along x-and y-directions (axes) by repeating its four times, which is called (4×4) supercell structure of h-BN bilayer is illustrated in figure-1(a). We have estimated the bond length between B-N atoms, interlayer distance between bilayer's atoms, binding energy, and ground state energy of bilayer h-BN supercell structure, they are found to be 1.43 Å, 3.72 Å, -707.36 meV & -874.39 Ry respectively. These values are comparable with other reported values of 2D materials [28,48]. They reflect that bilayer h-BN supercell structure is a stable material. The binding energy of bilayer h-BN is calculated by using equation-(1), [49];

$$(E_b)_d = E_{g(h-BN-bi)_d} - (E_{g(h-BN-mono)_d} + E_{g(h-BN-mono)_p}) \quad (1)$$

where, E_b, $E_{g(h\text{-}BN\text{-}bi)}$ & $E_{g(h\text{-}BN\text{-}monolayer)}$ represent the binding energy of h-BN system, ground state energy of h-BN bilayer supercell, and ground state energy of monolayer h-BN supercell structure respectively.

Furthermore, we have created the B atom vacancy defected h-BN (B-hBN), and N atom vacancy defected h-BN (N-hBN) materials by randomly removing single B atom, and single N atom from the upper surface of bilayer material respectively. Then calculate the minimum ground state, and binding energies of them. It is found that our considered materials (are shown in figures-1(b-c)) have minimum value of ground state energy, and maximum value of binding energy. The ground state energy, binding energy, defect formation energy, interlayer distance of bilayers, and bond length between B-N atoms of B-hBN are found to be -845.39 Ry, -515.36 meV, 0.21 eV, 3.72 Å & 1.46 Å respectively, and of N-hBN are found to be -831.69 Ry, -643.36 meV, 0.16 eV, 3.72 Å & 1.44 Å respectively. These calculated values are comparable with the reported values of others 2D materials [28, 48]. The binding energy of defected bilayer h-BN systems (B-hBN & N-hBN) are obtained by using equation-(2), [49];

$$E_b = E_{g(h-BN-bi)d} - \left(E_{g(w-hBN-mono)d} + E_{g(h-BN-mono)p} + E_{H2O}\right) \quad (2)$$

where, $(E_b)_d$, $E_{g(h\text{-}BN\text{-}bi)d}$, $E_{g(h\text{-}BN\text{-}mono)d}$ & $E_{g(h\text{-}BN\text{-}mono)p}$ are represented by binding energy of defected system, minimum ground state energy of B or N sites vacancy defected system, minimum ground state energy of B or N sites vacancy defected monolayer h-BN and minimum ground state energy of pristine h-BN monolayer respectively. The defect formation energy of defected bilayer h-BN systems (B-hBN & N-hBN) are obtained by using equation-(3), [14, 28, 41];

$$(E_d)_f = E_d - (E_p + n_B\mu_B + n_N\mu_N) \quad (3)$$

where, $(E_d)_f$, E_d, E_p, n_B or n_N & μ_B or μ_N represent the defect formation energy, ground state energy of defected monolayer of h-BN, ground state

energy of pristine monolayer of h-BN, number of defected atom and chemical potential of defected atom respectively. The calculations of above parameters implies that B-hBN & N-hBN are stable materials. From above estimated values of bond length between B-N atoms in structures, it is confirmed that pristine system is more compact than defected systems.

In addition, we have constructed water adsorption on B-hBN (w-B-hBN) and N-hBN (w-N-hBN) materials by adsorbing water molecule at different position (orientation) above the surface of defected layer of h-BN bilayer, and then relax calculation are done. It is found that adsorbed water molecule is appeared at 2.34 Å distance above from the upper surface of defected h-BN bilayer. The water molecules were then positioned on the left, middle, and right at constant 2.34 distances in various orientations above the upper surface of the defected h-BN bilayer. Their minimum ground state energy, binding energy, water adsorption energy, interlayer distance between the bilayers, and bond length between B-N atoms were then estimated. The calculated binding energies of the adsorbed water molecule at the left and right positions on the defective h-BN bilayer are found to be smaller than those of the middle location, while the ground state energy is found to be larger. Higher binding energies and lower ground state energies are known to indicate that a material is more stable. Thus, we have chosen w-B-hBN and w-N-hBN materials by adsorbing water molecule on the middle position at 2.34 Å distance above the surface of defected layer of h-BN bilayer for further calculations. The optimized and relax structures of water molecule adsorbed on the middle position at 2.34 Å distance above from the upper surface of defected h-BN bilayer (w-B-hBN & w-N-hBN) are shown in figures-1(d-e). The minimum ground state energy, binding energy, water adsorption energy, interlayer distance between the bilayers, and bond length between B-N atoms of w-B-hBN are found to be -880.04 Ry, -515.36 meV, -0.24 eV, 3.72 Å, and 1.46 Å respectively, and of w-N-hBN are found to be -867.393 Ry, -643.36 meV, -0.32 eV, 3.72 Å, and 1.44 Å respectively. These estimated values are agreed with the reported values of 2D materials [14, 28, 41, 50]. They reveal that these materials are stable materials. The binding energy of w-B-hBN & w-N-hBN are estimated by using equation-(4), [28, 41]

$$E_b = E_{g(w-hBN-bi)d} - \left(E_{g(w-hBN-mono)d} + E_{g(h-BN-mono)p} + E_{H2O}\right) \quad (4)$$

where, E_b, $E_{g(w\text{-}hBN\text{-}bi)d}$, $E_{g(w\text{-}hBN\text{-}mono)d}$, $E_{g(h\text{-}BN\text{-}mono)p}$ & E_{H2O} are represented by binding energy w-B-hBN or w-N-hBN system, minimum ground state energy w-B-hBN or w-N-hBN, minimum ground state energy of water adsorbed on B or N sites h-BN monolayer, minimum ground state energy of pristine h-BN monolayer and ground state energy of water molecule respectively. We also have compared the estimated parameters of considered systems and found that pristine h-BN bilayer supercell structure is more compact and stable than defected, and water adsorption on defected materials. Pristine bilayer h-BN, B-hBN, N-hBN, w-B-hBN & w-N-hBN bilayer supercell structures are shown in figures-1(a-e) respectively.

3.2 Electronic Properties

Electronic properties of pristine h-BN, single B atom vacancy defect on h-BN (B-hBN), single N atom vacancy defect on h-BN (N-hBN), water adsorption on B-hBN (w-B-hBN) & water adsorption on N-hBN (w-N-hBN) bilayer supercell materials are studied by the analysis of their band structures and density of states (DoS) plots. The band structure plots of these materials are shown in figures-2(a-e) respectively.

In the band plots, highly symmetric points ($\Gamma - M - K - \Gamma$) within the irreducible Brillion zone (BZ) are plotted along the x-axis, and its corresponding energy levels are plotted along the y-axis. The horizontal blue dot line represents the Fermi energy level which separates the electronic bands. The region below the Fermi energy level is called valence band, and above the Fermi energy level is called conduction band. To obtain the fine band structure, we have taken 200 k-points in the irreducible BZ. Bandgap energy is the distance between the material's lowest level of conduction band and topmost level of valence band. The pristine bilayer h-BN supercell structure's bandgap energy 4.56 eV is calculated, which indicates that material has a broad bandgap. This number is somewhat consistent with the monolayer h-BN supercell structure value that has been reported [15, 28]. Figure-1(a) depicts the pristine bilayer h-BN supercell structure's electronic band states that we have obtained. Compared to conduction band states, valence band states are found to be more closely spaced with the Fermi energy level in band structure. Consequently, we have p-type Schottky barrier of pristine bilayer h-BN supercell structure.

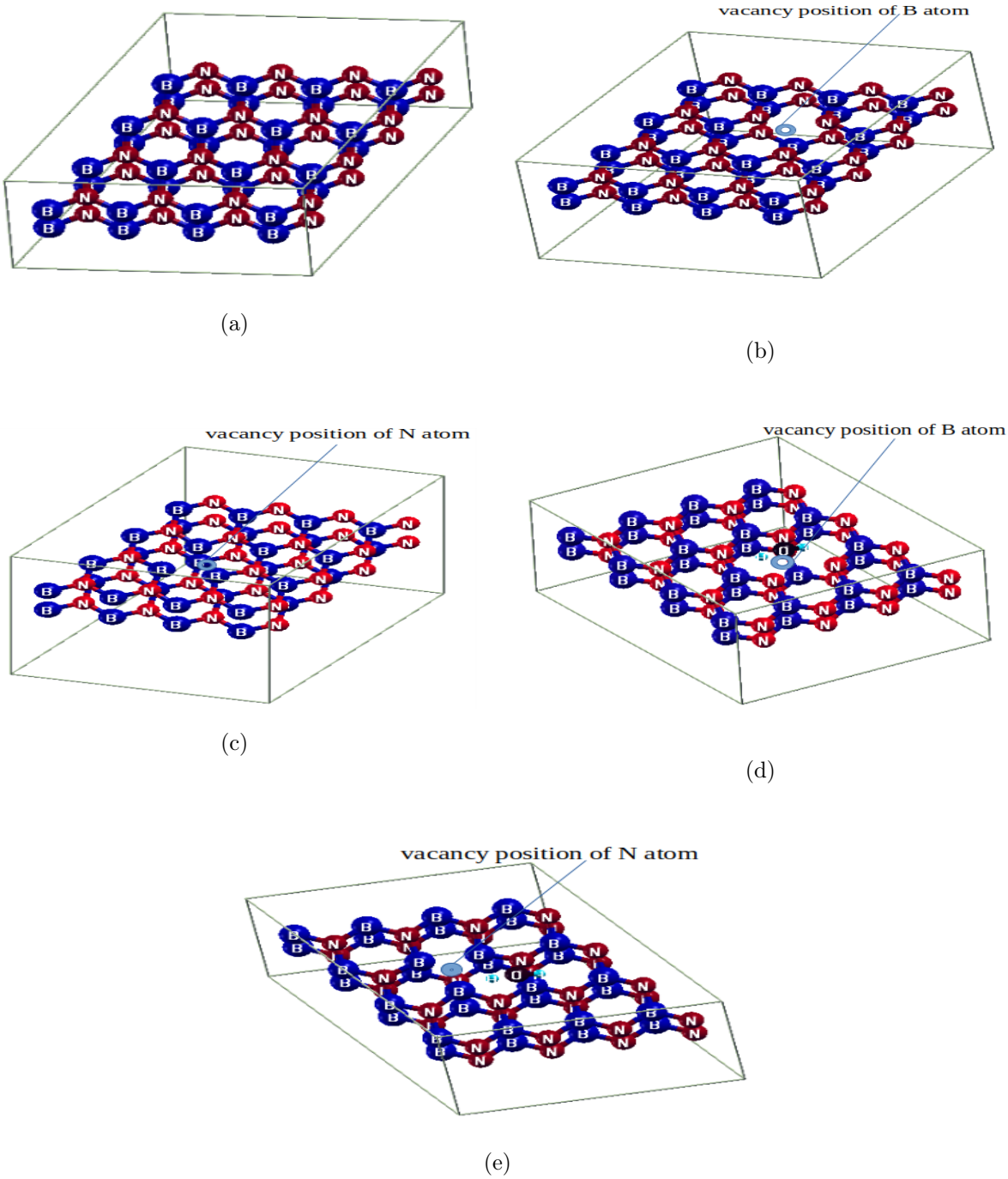

Figure 1: (Color online) Optimized and relax structures of B N sites vacancy defected bilayer h-BN supercell material: (a) pristine bilayer h-BN supercell structure, (b) single Boron atom vacancy defected bilayer h-BN supercell (B-hBN) material, (c) single Nitrogen atom vacancy defected h-BN bilayer supercell (N-hBN) material, (d) water adsorption on B-hBN (i.e., w-B-hBN) material, and (e) water adsorption on N-hBN (i.e., w-N-hBN) material.

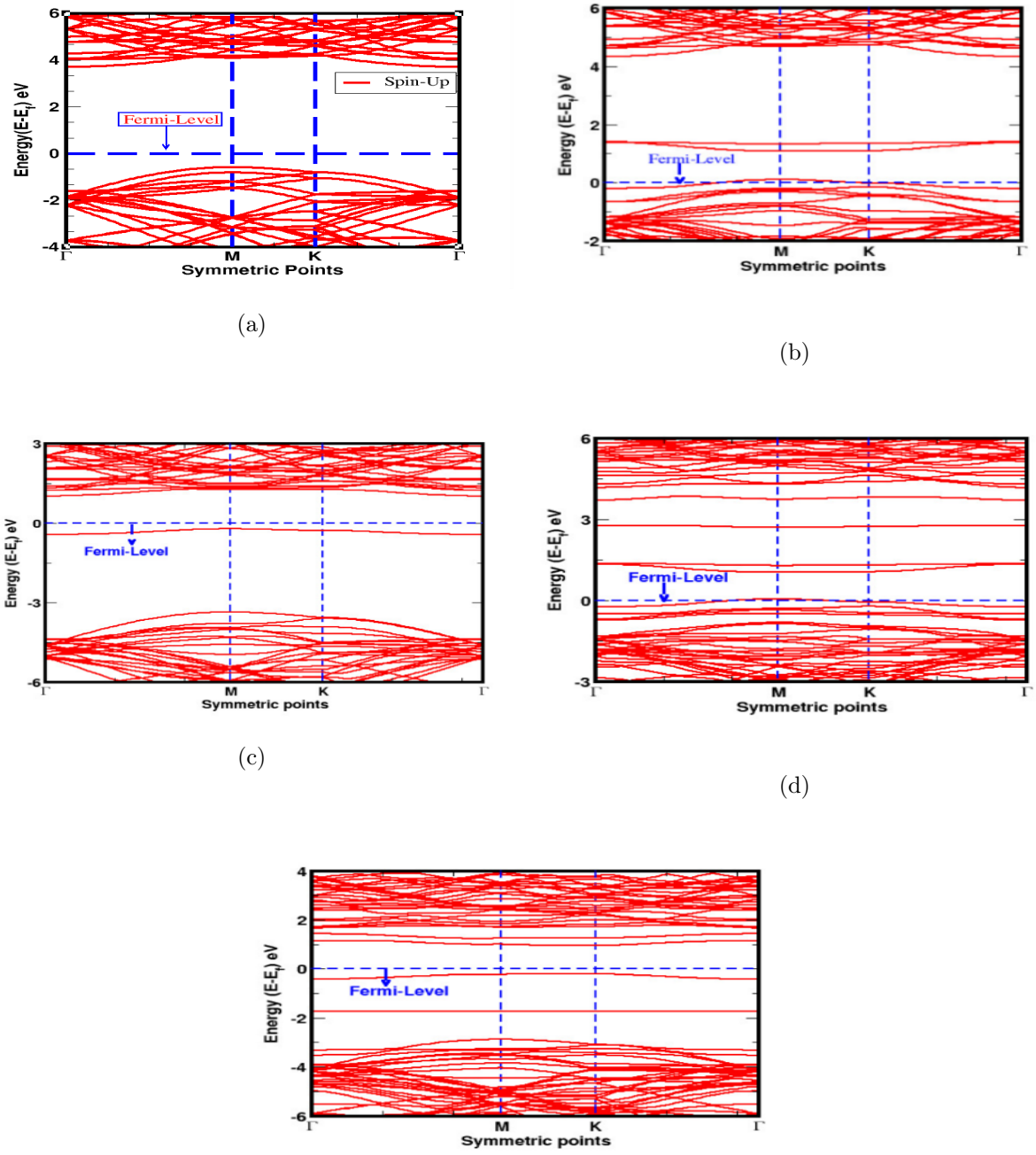

Figure 2: (Colour online) band structure plots of pristine and defected bilayer h-BN materials: (a) band structure of pristine h-BN bilayer supercell material, (b) band structure of B-hBN bilayer supercell material, (c) band structure of N-hBN bilayer supercell material, (d) band structure of w-B-hBN bilayer supercell material, and (e) band structure of w-N-hBN bilayer supercell material.

Figures-2(b-c) display the band structures that we have created of B-hBN & N-hBN materials, respectively. It is calculated that the bandgap energies of B-hBN & N-hBN are 1.25 eV & 1.49 eV, respectively. The energy gaps between the Fermi energy level and the lowest level of band states in the conduction band, and the Fermi level and higher level of band states in the valence band are added up to get these values. Electronic band states of valence band are observed near the Fermi energy level in both materials. Thus, they are known as p-type semiconducting materials. The unpaired arrangement of electronic spin-states in the atoms' orbitals within the structures is what causes the flat bands to form in the valence band of N-hBN and the conduction band of B-hBN.

Moreover, we have analyzed the band structures of w-B-hBN & w-N-hBN materials, which are il-

lustrated in figures-2(d-e) respectively. From these plots, we have estimated the bandgap energy of w-B-hBN & w-N-hBN are found to be 0.97 eV & 1.24 eV respectively. It means, adsorbed water molecule affects the electronic states of defected systems. This is because, water molecule like to be adsorbed on the region of vacancy sites, as a result, more numbers of flat bands are appeared in the conduction band of w-B-hBN & in the valence band of w-N-hBN materials. In both materials, electronic band states of valence band are presented closely with the Fermi energy level, and hence, they are p-type semiconducting materials. The estimated values of total minimum ground state energy, Fermi energy, bandgap energy, binding energy, defect formation energy of studied materials are presented in Table-1.

Table 1: Estimated values of total energy (E_t), Fermi energy (E_f), band gap energy (E_g), binding energy (E_b), and defect formation energy (E_d) of pristine h-BN, B-hBN, N-hBN, w-B-hBN & w-N-hBN bilayer supercell materials.

Bilayer materials	E_t **(Ry)**	E_f **(eV)**	E_g **(eV)**	E_b **(meV)**	E_d **(eV)**	**Nature of material**
h-BN	-852.38	-2.27	4.56	-707.36	-	Wide bandgap
B-hBN	-845.39	-2.93	1.25	-515.36	0.21	Semiconductor
N-hBN	-831.69	-0.38	1.49	-643.36	0.16	Semiconductor
w-B-hBN	-880.04	-3.07	0.97	-515.36	-	Semiconductor
w-N-hBN	-867.39	-0.60	1.24	-643.36	-	Semiconductor

In addition, we have analyzed the DoS plots of pristine h-BN, B-hBN, N-hBN, w-B-hBN & w-N-hBN bilayer supercell materials for the investigation of their electronic properties. The DoS plots of these materials are shown in figures-3(a-e) respectively, where DoS states are plotted along y-axis and corresponding it energies are taken along x-axis. The vertical dot line separates the valence band and conduction band. The region toward LHS represents valence band, and region toward RHS represents conduction band. The horizontal dot line distinguishes the DoS states of up-spins and down-spins. Black and red colours of spin states are respectively, indicate the distributed up and down spin-states of electrons in the orbitals of atoms present in the materials. It is found that bandgap energies of pristine h-BN, B-hBN, N-hBN, w-B-hBN & w-N-hBN bilayer supercell materials have values 4.56 eV, 1.30 eV, 1.47 eV, 1.27 eV & 1.12 eV respectively. These calculated values are fairly agreed with the computed values obtained from band structure calculations [5, 28]. Thus, it is also confirmed that pristine h-BN bilayer supercell is a wide bandgap material, and B-hBN, N-hBN, w-B-hBN & w-N-hBN bilayer supercell structures have semiconducting nature. Semiconducting materials can find usage in a variety of technologies, including memory devices, photocatalysts, integrated logic circuits, transistors, signal amplifiers, photodetectors, flexible optoelectronic devices, solar cells [9, 13, 17].

3.3 Magnetic Properties

Magnetic properties of pristine h-BN, B-hBN, N-hBN, w-B-hBN & w-N-hBN bilayer supercell materials are investigated by the analysis of their density of states (DoS) and partial density of states (PDoS) calculations. DoS gives an idea of number of electronic states per unit energy range, and PDoS gives an idea of distribution of spin states of electrons in the orbital of atom present in the material [15, 23, 26]. DoS & PDoS plots of pristine h-BN, B-hBN, N-hBN, w-B-hBN & w-N-hBN materials are presented in the figures-3(a-e) & figures-4(a-e) respectively. In DoS & PDoS plots, vertical dot line represents the Fermi energy level which separates the electronic bands. The horizontal dot line separates the distributed up-and down-spin states.

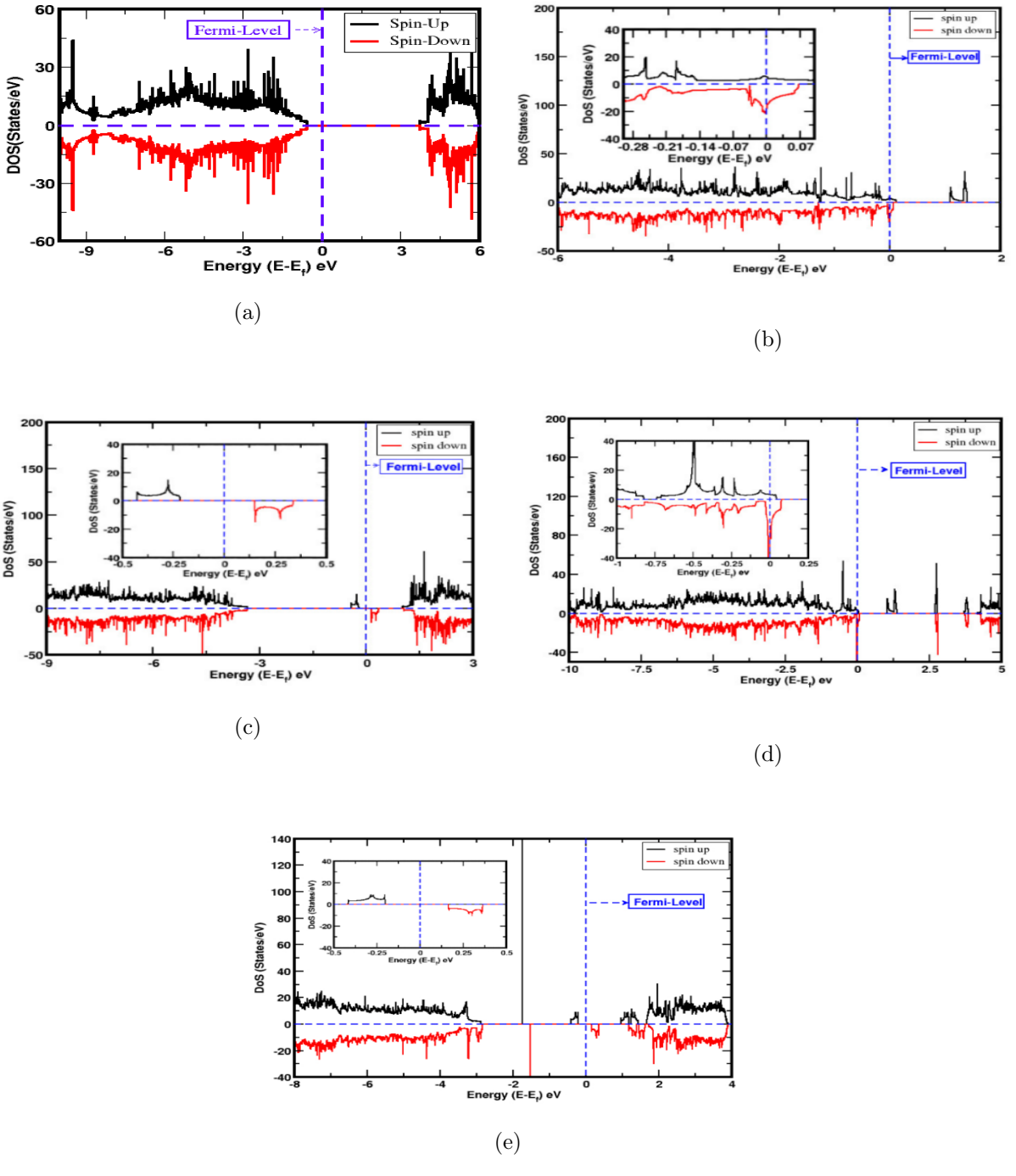

Figure 3: Colour online) density of states (DoS) plots of pristine and defected bilayer h-BN materials: (a) DoS plot of pristine h-BN bilayer supercell material, (b) DoS plot of B-hBN bilayer supercell material, (c) DoS plot of N-hBN bilayer supercell material, (d) DoS plot of w-B-hBN bilayer supercell material, and (e) DoS plot of w-N-hBN bilayer supercell material. Insets represent the zoom scale of DoS plots.

The DoS & PDoS plots of pristine h-BN bilayer supercell structure are shown in figure-3(a) & figure-4(a) respectively. In both plots, up and down spin states are symmetrically distributed around the Fermi energy level. It indicates that magnetic moment has not yet developed. It is therefore a non-magnetic substance. We have examined the DoS & PDoS plots of B-hBN & N-hBN materials, which are depicted in figures-3(b-c) & figures-4(b-c) respectively. Asymmetric distribution of up and down spin states of electrons in atom orbitals in materials around the Fermi energy level results in magnetic moments of -1.71 μB/cell in B-hBN & 1.00 μB/cell in N-hBN. As a result, both materials possess magnetic properties. The negative sign signified that down spin states of electrons contribute more than up spin states of electrons to the formation of magnetic moment in the materials. Based

on the calculations, we found that the magnetic moment values of B atom's 2s & 2p orbitals are 0.01 µB/cell & -0.06 µB/cell, whereas N atom's 2s & 2p orbitals have 0.14 µB/cell & -1.52 µB/cell in B-hBN. It has been demonstrated that the N atom's 2p orbital plays a major role in the magnetic moment produced in B-hBN material. In the same way, we calculated the magnetic moment of N-hBN material and found that it is 0.04 µB/cell & 0.30 µB/cell of B atoms' 2s & 2p orbitals, and 0.08 µB/cell & 0.58 µB/cell of N atoms' 2s & 2p orbitals, respectively. Positive magnetic moment values show that up spin states are mostly responsible for the material's magnetic moment production.

2

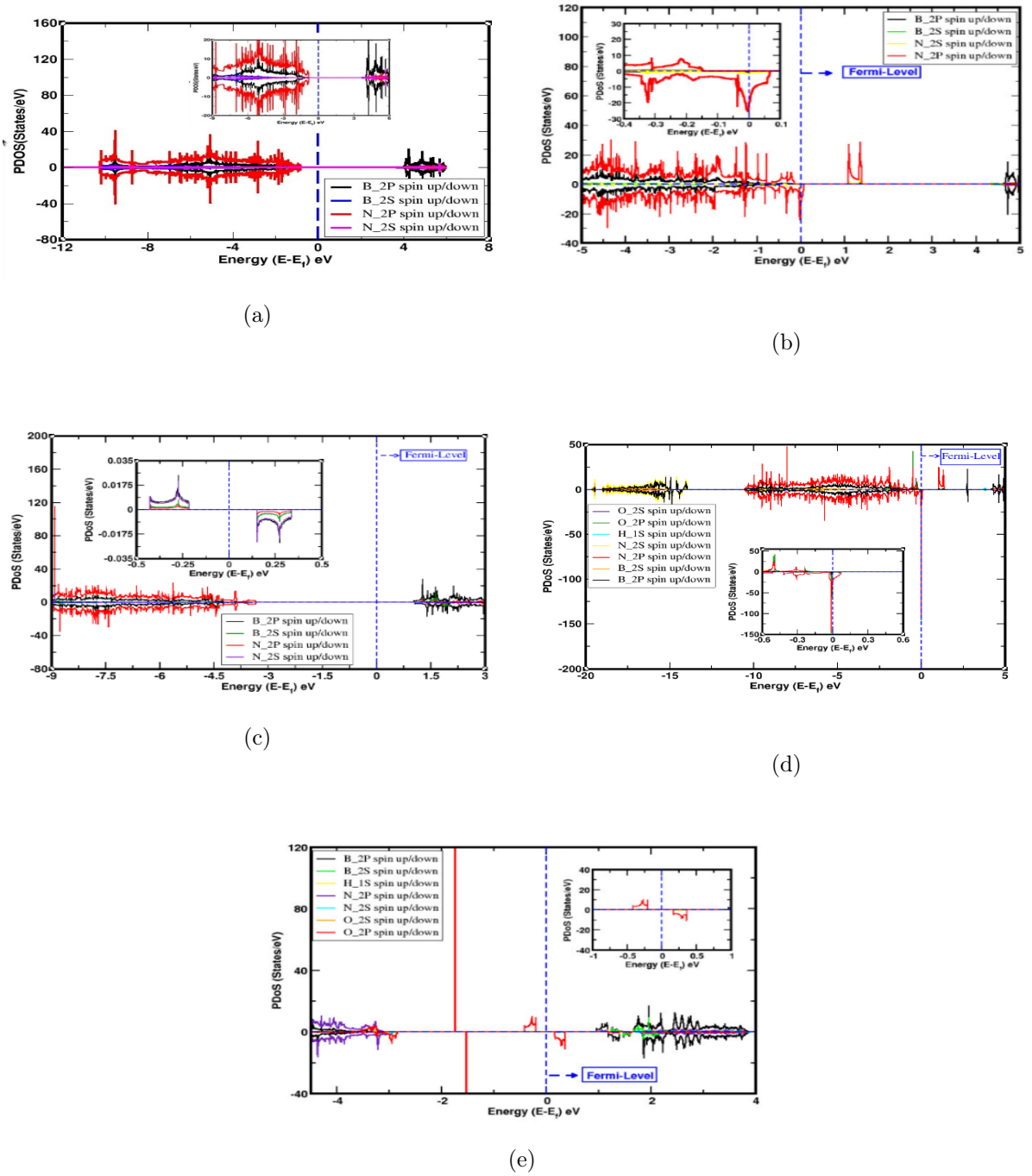

Figure 4: (Colour online) Partial density of states (PDoS) plots of pristine and defected bilayer h-BN materials: (a) PDoS plot of pristine h-BN bilayer supercell material, (b) PDoS plot of B-hBN bilayer supercell material, (c) PDoS plot of N-hBN bilayer supercell material, (d) PDoS plot of w-B-hBN bilayer supercell material, and (e) PDoS plot of w-N-hBN bilayer supercell material. Insets represent the zoom

scale of PDoS plots.

Furthermore, we have examined the DoS & PDoS computations of w-B-hBN & w-N-hBN bilayer supercell materials to learn more about their magnetic characteristics. Figures-3(d-e) and figures-4(d-e) respectively depict the asymmetric distribution of up and down spin states of electron in the orbitals of atoms found in the materials near the Fermi energy level. It indicates that they possess magnetic properties. We have estimated the magnetic moment created by the unpaired spin states of electrons in the orbitals of atoms present in the materials. In w-B-hBN, the spins in the 2s & 2p orbitals of B atoms and the 2s & 2p orbitals of N atoms have values of 0.01 μ_B/cell & 0.57 μ_B/cell, and -0.24 μ_B/cell & -1.69 μ_B/cell, respectively. Additionally, the magnetic moments of the 1s of H atoms and 2s & 2p of O atom in w-B-hBN material are found to be -0.02 μ_B/cell, and 0.00 µB/cell & 0.37 μ_B/cell respectively. The total magnetic moment generated in w-B-hBN is therefore equal to -1.00 μ_B/cell. Likewise, we computed the magnetic moment given by unpaired spin states in the 2s & 2p orbitals of B atoms, and 2s & 2p orbitals of N atoms are found to be 0.04 μ_B/cell & 0.00 μ_B/cell, and 0.00 μ_B/cell & -0.42 μ_B/cell in w-N-hBN martial respectively. Also, magnetic moment given by spin states of electrons in the 1s orbital of H atoms and 2s & 2p orbitals of O atom in w-N-hBN material are found to be 0.00 μ_B/cell, and 0.00 μ_B/cell & 1.38 μ_B/cell values respectively. This indicates that the formation of magnetic moment in the material is primarily attributed to the 2p orbital of N & O atoms. Consequently, total magnetic moment of w-N-hBN material have value -1.00 µB/cell. The estimated magnetic moment of B-hBN, N-hBN, w-B-hBN & w-N-hBN materials are illustrated in Table-2.

Table 2: Magnetic moment (μ_T in μ_B/cell) is produced by unpaired spin states of electrons in the 2s & 2p orbitals of Boron, Nitrogen, and Oxygen atoms and 1s orbital of Hydrogen atom in the pristine, defected, and water adsorbed on defected h-BN bilayer supercell structures.

Orbitals	**Materials**			
	B-hBN	w-B-hBN	N-hBN	w-N-hBN
2s of B atoms	0.01	0.01	0.04	0.04
2p of B atoms	-0.06	0.57	0.30	-0.00
2s of N atoms	-0.14	-0.24	0.08	-0.00
2p of N atoms	-1.52	-1.69	0.58	-0.42
1s of H atoms	-	-0.02	-	0.00
2s of O atom	-	0.00	-	0.00
2p of O atom	-	0.37	-	1.38
Total magnetic moment (μ_T)	-1.71	-1.00	1.00	1.00

It can be observed from the calculations above that B & N vacancy defected atoms turn non-magnetic pure h-BN bilayer supercell structures into magnetic ones. This is because the electrons in the remaining atoms in the structures have rearranged their unpaired spin states. However, because the unpaired electron spins around the B vacancy position in the h-BN structure are rearranged together with the adsorbed water molecule, the presence of adsorbed water on B sites h-BN weakens the magnetic moment. Furthermore, the values of the magnetic moment of N vacancy defected h-BN, and water adsorbed on the vacancy defective h-BN of N sites are comparable. These values are produced in the materials as a result of the electronic spin states' unpaired configuration. We determined the magnetic moment values in h-BN materials with vacancy defects at sites B and N. These materials appear to be promising for use in a variety of devices requiring magnetic characteristics because of the appearance of magnetism. Magnetism and magnetic materials are essential to many of the modern electronic equipment we use. Biomedicine, molecular biology, biochemistry, diagnostics, catalysis, and nanoelectronics devices are just a few of the industrial applications for novel nanomagnetic materials that could be used. Other applications include magnetic seals in motors, magnetic sensors, bank check ink, electrical power generators and transformers, magnetic recording media, computers, and more [51, 52]. Therefore, key frameworks for the material to device applications may be provided by our understanding of unique electrical and magnetic phenomena on defective materials.

4 Conclusion

In the present work, we have studied the impact of adsorbed water molecule on single B atom vacancy defect on h-BN, single N atom vacancy de-

fect on h-BN by first-principles calculation based on spin-polarized DFT methods through Quantum ESPRESSO (QE) computational tools. Firstly, we have investigated the structural properties of 2D bilayer hexagonal-Boron Nitride (h-BN), single B atom vacancy defect on h-BN (B-hBN), single N atom vacancy defect on h-BN (N-hBN), water adsorption; on B-hBN (w-B-hBN) and on N-hBN (w-N-hBN), materials by estimating their ground states energy and binding energy. They are found to be structurally stable materials. Additionally, we have measured the interlayer distances and bond length between any two nearest B-N atoms, and found that defective materials are also shown to be less compact than perfect h-BN bilayer material. Secondly, we have studied the electronic properties of considered materials by developing their band structures and DoS plots. It is found that pristine h-BN has wide bandgap energy of value 4.56 eV, so is called wide bandgap material. On the other hands, B-hBN, N-hBN, w-B-hBN & w-N-hBN materials have small bandgap energy of values 1.25 eV, 1.49 eV, 0.97 eV & 1.24 eV respectively. Hence, they have semiconducting properties. Thirdly, we have examined the magnetic properties of pristine h-BN, B-hBN, N-hBN, w-B-hBN & w-N-hBN bilayer supercell materials, by the analysis of their DoS and PDoS calculations. Electronic spin-states of up and down spins are symmetrically distributed around the Fermi energy level in pristine h-BN, and hence it has zero value of magnetic moment. So, it is a non-magnetic material. The distribution of up and down spins is asymmetrically distributed around the Fermi energy level in B-hBN, N-hBN, w-B-hBN & w-N-hBN materials. As a results, magnetic moment are developed of values -1.71 μ_B/cell, 1.00 μ_B/cell, -1.00 μ_B/cell & 1.00 μ_B/cell respectively. Thus, B & N sites vacancy defected h-BN, and water adsorption on these defected materials are magnetic materials. Thus, water adsorption on vacancy defected h-BN materials, and vacancy defects on pristine h-BN materials cause it to become magnetic instead of non-magnetic. They might be useful in the field of applications for devices.

Authorship Contribution Statement

M. Nepal: Gathering information, analyzing and interpreting it, making figures and graphs, and writing the manuscript.
G. Poudel: Gathering information, assisting with data analysis.
S. Aryal & A. Devkota: Gathering data and contributing to its analysis.
H. K. Neupane: Developed the idea, oversaw its analysis, interpreted the findings, and thoroughly revised the manuscript.

Data Availability

If you have any questions about data reproduction, you can get the data that were used to create the figures, tables, and graphs in this paper directly from the corresponding author.

Declaration of Competing Interest

The authors declare that none of the work reported in this study could have been influenced by any known competing financial interests or personal relationships.

Acknowledgments

The authors acknowledge the condensed matter research lab CDP TU, TWAS research funds RG 20-316, network project NT-14 of ICTP/OE for the computing capacity, and Prof. Narayan Prasad Adhikari for his excellent input in reviewing the paper.

References

[1] L. Kleinman and J. C. Phillips. Crystal potential and energy bands of semiconductors. ii. self-consistent calculations for cubic boron nitride. *Phys. Rev.*, 117(2):460–464, 1960.

[2] P. J. Gielisse, S. S. Mitra, J. N. Plendl, R. D. Griffis, L. C. Mansur, R. Marshall, and E. A. Pascoe. Lattice infrared spectra of boron nitride and boron monophosphide. *Phys. Rev.*, 155(3):1039–1046, 1967.

[3] Y. F. Tsay, A. Vaidyanathan, and S. S. Mitra. Electronic structure and optical properties of cubic bn. *Phys. Rev. B*, 19(10):5422–5428, 1979.

[4] A. Zunger, A. Katzir, and A. Halperin. Optical properties of hexagonal boron nitride. *Phys. Rev. B*, 13(12):5560–5573, 1976.

[5] H. K. Neupane and N. P. Adhikari. First-principles study of defected single layer hexagonal boron-nitride (h-bn). *Nepal Journal of Science and Technology*, 20(2):55–66, 2021.

[6] S. Larach and R. E. Shrader. Electroluminescence from boron nitride. *Phys. Rev.*, 102(2):582–582, 1956.

[7] S. Lousinian, N. Kalfagiannis, and S. Logothetidis. Optical and surface characterization of amorphous boron nitride thin films for use as blood compatible coatings. *Solid State Sci.*, 11(10):1801–1805, 2009.

[8] Z. Li and F. Gao. Structure, bonding, vibration and ideal strength of primitive-centered tetragonal boron nitride. *Phys. Chem. Chem. Phys.*, 14(2):869–876, 2012.

[9] N. Zhang, H. Liu, H. Kan, X. Wang, H. Long, and Y. Zhou. The preparation of high-adsorption, spherical, hexagonal boron nitride by template method. *J. Alloys Compd.*, 613:74–79, 2014.

[10] J. Wang, F. Ma, and M. Sun. Graphene, hexagonal boron nitride, and their heterostructures: properties and applications. *RSC Adv.*, 7(27):16801–16822, 2017.

[11] B. Arnaud, S. Lebègue, P. Rabiller, and M. Alouani. Huge excitonic effects in layered hexagonal boron nitride. *Phys. Rev. Lett.*, 96(2):026402, 2006.

[12] J. Olander and K. Larsson. Initial growth of hexagonal and cubic boron nitride: A theoretical study. *Phys. Rev. B*, 68(7):075411, 2003.

[13] Y. Lin and J. W. Connell. Advances in 2d boron nitride nanostructures: nanosheets, nanoribbons, nano meshes, and hybrids with graphene. *Nanoscale*, 4(22):6908–6939, 2012.

[14] H. K. Neupane and N. P. Adhikari. First-principles study of structure, electronic, and magnetic properties of c sites vacancy defects in water adsorbed graphene/mos2 van der waals heterostructures. *J. Mol. Model.*, 27(3):82, 2021.

[15] H. K. Neupane and N. P. Adhikari. Tuning structural, electronic, and magnetic properties of c sites vacancy defects in graphene/mos2 van der waals heterostructure materials: A first-principles study. *Adv. Condens. Matter Phys.*, pages 1–11, 2020.

[16] H. K. Neupane and N. P. Adhikari. Structural, electronic and magnetic properties of s sites vacancy defects graphene/mos2 van der waals heterostructures: First-principles study. *Int. J. Comput. Mater. Sci. Eng.*, 10(02):2150009, 2021.

[17] Y. Tian, X. Pan, Y. Liu, and J. Zhao. Theoretical study of the adsorption of cho radicals on hexagonal boron nitride sheet: Structural and electronic changes. *Appl. Surf. Sci.*, 295:137–143, 2014.

[18] J. Zhao and Y. Ding. Theoretical investigation of the divacancies in boron nitride nanotubes: properties and surface reactivity toward various adsorbates. *J. Chem. Phys.*, 131(1):2023, 2009.

[19] R. Wang, D. Zhang, and C. Liu. The germanium-doped boron nitride nanotube serving as a potential resource for the detection of carbon monoxide and nitric oxide. *Comput. Mater. Sci.*, 82:361–366, 2014.

[20] Y. Zhang, L. Tao, C. Xie, D. Wang, and S. Wang. Defect engineering on electrode materials for rechargeable batteries. *Adv. Mater.*, 32(7):1905923, 2020.

[21] C. Kittel. *Introduction to Solid State Physics*. John Wiley & Sons, Inc, 2005.

[22] O. V. Yazyev and L. Helm. Defect-induced magnetism in graphene. *Phys. Rev. B*, 75(12):125408, 2007.

[23] H. K. Neupane and N. P. Adhikari. Structure, electronic and magnetic properties of 2d graphene-molybdenum disulphide (g-mos2) heterostructure (hs) with vacancy defects at mo sites. *Comput. Condens. Matter*, 24:e00489, 2020.

[24] C. F. Pupim, A. J. L. Catão, and A. López-Castillo. Boron–nitrogen dative bond. *J. Mol. Model.*, 24(10):283, 2018.

[25] R. J. Cava, H. Ji, M. K. Fuccillo, Q. D. Gibson, and Y. S. Hor. Crystal structure and chemistry of topological insulators. *J. Mater. Chem. C*, 1(19):3176–3189, 2013.

[26] A. Ramasubramaniam, D. Naveh, and E. Towe. Tunable band gaps in bilayer graphene-bn heterostructures. *Nano Lett.*, 11(3):1070–1075, 2011.

[27] G. J. Slotman, M. M. Van Wijk, P. L. Zhao, A. Fasolino, M. I. Katsnelson, and S. Yuan. Effect of structural relaxation on the electronic structure of graphene on hexagonal boron nitride. *Phys. Rev. Lett.*, 115(18):186801, 2015.

[28] H. K. Neupane and N. P. Adhikari. Effect of vacancy defects in 2d vdw graphene/h-bn heterostructure: First-principles study. *AIP Adv.*, 11(8), 2021.

[29] J. Wang, F. Ma, W. Liang, and M. Sun. Electrical properties and applications of graphene, hexagonal boron nitride (h-bn), and graphene/h-bn heterostructures. *Mater. Today Phys.*, 2:6–34, 2017.

[30] S. Zhu, J. Cheng, Z. Qiao, and J. Yang. High temperature solid-lubricating materials: A review. *Tribol. Int.*, 133:206–223, 2019.

[31] G. Giovannetti, P. A. Khomyakov, G. Brocks, P. J. Kelly, and J. van den Brink. Electronic structure: Wide-band, narrow-band, and strongly correlated systems-substrate-induced band gap in graphene on hexagonal boron nitride: Ab initio density functional. *Phys. Rev.-Sect. B-Condens. Matter*, 76(7):73103, 2007.

[32] C. Zhi, Y. Bando, C. Tang, H. Kuwahara, and D. Golberg. Large-scale fabrication of boron nitride nanosheets and their utilization in polymeric composites with improved thermal and mechanical properties. *Adv. Mater.*, 21(28):2889–2893, 2009.

[33] H. Zhou, J. Zhu, Z. Liu, Z. Yan, and J. M. Tour. High thermal conductivity of suspended few-layer hexagonal boron nitride sheets. *Nano Res.*, 7(8):1232–1240, 2014.

[34] I. Jo, M. T. Pettes, J. Kim, K. Watanabe, T. Taniguchi, Z. Yao, and L. Shi. Thermal conductivity and phonon transport in suspended few-layer hexagonal boron nitride. *Nano Lett.*, 13(2):550–554, 2013.

[35] C. C. Chen, Z. Li, L. Shi, and S. B. Cronin. Thermoelectric transport across graphene/hexagonal boron nitride/graphene heterostructures. *Nano Res.*, 8(2):666–672, 2015.

[36] W. Zhou, S. Qi, Q. An, H. Zhao, and N. Liu. Thermal conductivity of boron nitride reinforced polyethylene composites. *Mater. Res. Bull.*, 42(10):1863–1873, 2007.

[37] W. Bououden, Y. Benguerba, A. S. Darwish, A. Attoui, and I. M. Alnashef. Surface adsorption of crizotinib on carbon and boron nitride nanotubes as anti-cancer drug carriers: Cosmo-rs and dft molecular insights. *J. Mol. Liq.*, 338:116666, 2021.

[38] A. Nakhli, M. Bergaoui, K. H. Toumi, M. Khalfaoui, and A. Erto. Molecular insights through computational modeling of methylene blue adsorption onto low-cost adsorbents derived from natural materials: A multi-model's approach. *Comput. Chem. Eng.*, 140:106965, 2020.

[39] A. S. Darwish, S. E. Warrag, T. Lemaoui, M. K. Alseiari, and N. Alamoodi. Green extraction of volatile fatty acids from fermented wastewater using hydrophobic deep eutectic solvents. *Fermentation*, 7(4):226, 2021.

[40] S. Benabid, A. F. Streit, Y. Benguerba, G. L. Dotto, A. Erto, and B. Ernst. Molecular modeling of anionic and cationic dyes adsorption on sludge derived activated carbon. *J. Mol. Liq.*, 289:111119, 2019.

[41] H. K. Neupane and N. P. Adhikari. Adsorption of water on c sites vacancy defected graphene/h-bn: First-principles study. *J. Mol. Model.*, 28(4):107, 2022.

[42] W. Kohn and L. J. Sham. Self-consistent equations including exchange and correlation effects. *Phys. Rev.*, 140(4A):A1133–A1138, 1965.

[43] J. P. Perdew, K. Burke, and M. Ernzerhof. Generalized gradient approximation made simple. *Phys. Rev. Lett.*, 77(18):3865–3868, 1996.

[44] B. G. Pfrommer, M. Côté, S. G. Louie, and M. L. Cohen. Relaxation of crystals with the quasi-newton method. *J. Comput. Phys.*, 131(1):233–240, 1997.

[45] S. Grimme, J. Antony, S. Ehrlich, and H. Krieg. A consistent and accurate ab initio parametrization of density functional dispersion correction (dft-d) for the 94 elements h-pu. *J. Chem. Phys.*, 132(15), 2010.

[46] N. Marzari, D. Vanderbilt, A. De Vita, and M. C. Payne. Thermal contraction and disordering of the al (110) surface. *Phys. Rev. Lett.*, 82(16):3296–3299, 1999.

[47] H. J. Monkhorst and J. D. Pack. Special points for brillouin-zone integrations. *Phys. Rev. B*, 13(12):5188–5192, 1976.

[48] B. Chettri, P. K. Patra, T. V. Vu, C. Q. Nguyen, and D. P. Rai. Induced ferromagnetism in bilayer hexagonal boron nitride (h-bn) on vacancy defects at b and n sites. *Phys. E Low-Dimens. Syst. Nanostructures*, 126:114436, 2021.

[49] T. V. Vu, N. V. Hieu, H. V. Phuc, N. N. Hieu, and C. V. Nguyen. Graphene/wsete van der waals heterostructure: Controllable electronic properties and schottky barrier via interlayer coupling and electric field. *Applied Surface Science*, 507:145036, 2020.

[50] Q. Peng, Z. Guo, B. Sa, J. Zhou, and Z. Sun. New gallium chalcogenides/arsenene van der waals heterostructures promising for photocatalytic water splitting. *International Journal of Hydrogen Energy*, 43(33):15995–16004, 2018.

[51] M. V. Makarova, Y. Akaishi, T. Ikarashi, K. S. Rao, S. Yoshimura, and H. Saito. Alternating magnetic force microscopy: effect of si doping on the temporal performance degradation of amorphous fecob magnetic tips. *Journal of Magnetism and Magnetic Materials*, 471:209–214, 2019.

[52] H. X. Peng, F. Qin, and M. H. Phan. *Ferromagnetic Microwire Composites: from Sensors to Microwave Applications*. Springer, 2016.